

## Article

# NiCoAl-Based Monolithic Catalysts for the N<sub>2</sub>O Intensified Decomposition: A New Path towards the Microwave-Assisted Catalysis

Olga Muccioli <sup>1</sup>, Eugenio Meloni <sup>1,\*</sup>, Simona Renda <sup>1,\*</sup>, Marco Martino <sup>1</sup>, Federico Brandani <sup>2</sup>,  
Pluton Pullumbi <sup>2</sup> and Vincenzo Palma <sup>1</sup>

<sup>1</sup> Department of Industrial Engineering, University of Salerno, Via Giovanni Paolo II 132, 84084 Fisciano, Italy; omuccioli@unisa.it (O.M.)

<sup>2</sup> Air Liquide, Paris Innovation Campus, 1 Chemin de la Porte des Loges, 78350 Les Loges en Josas, France

\* Correspondence: emeloni@unisa.it (E.M.); srenda@unisa.it (S.R.)

**Abstract:** Nitrous oxide (N<sub>2</sub>O) is considered the primary source of NO<sub>x</sub> in the atmosphere, and among several abatement processes, catalytic decomposition is the most promising. The thermal energy necessary for this reaction is generally provided from the external side of the reactor by burning fossil fuels. In the present work, in order to overcome the limits related to greenhouse gas emissions, high heat transfer resistance, and energy losses, a microwave-assisted N<sub>2</sub>O decomposition was studied, taking advantages of the microwave's (MW) properties of assuring direct and selective heating. To this end, two microwave-susceptible silicon carbide (SiC) monoliths were layered with different nickel–cobalt–aluminum mixed oxides. Based on the results of several characterization analyses (SEM/EDX, BET, ultrasound washcoat adherence tests, Hg penetration technique, and TPR), the sample showing the most suitable characteristics for this process was reproduced in the appropriate size to perform specific MW-assisted catalytic activity tests. The results demonstrated that, by coupling this catalytic system with an opportunely designed microwave heated reactor, it is possible to reach total N<sub>2</sub>O conversion and selectivity of a highly concentrated N<sub>2</sub>O stream (50 vol%) at T = 550 °C, the same required in the conventionally heated process to remove N<sub>2</sub>O from a less concentrated gas stream (20 vol%).

**Keywords:** N<sub>2</sub>O decomposition; structured catalysts; microwave heating; silicon carbide monoliths; process intensification; alternative heating; electrification



**Citation:** Muccioli, O.; Meloni, E.; Renda, S.; Martino, M.; Brandani, F.; Pullumbi, P.; Palma, V. NiCoAl-Based Monolithic Catalysts for the N<sub>2</sub>O Intensified Decomposition: A New Path towards the Microwave-Assisted Catalysis.

*Processes* **2023**, *11*, 1511. <https://doi.org/10.3390/pr11051511>

Academic Editor: Albert Renken

Received: 18 April 2023

Revised: 2 May 2023

Accepted: 12 May 2023

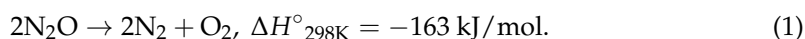
Published: 16 May 2023



**Copyright:** © 2023 by the authors. Licensee MDPI, Basel, Switzerland. This article is an open access article distributed under the terms and conditions of the Creative Commons Attribution (CC BY) license (<https://creativecommons.org/licenses/by/4.0/>).

## 1. Introduction

Nitrous oxide (N<sub>2</sub>O) is considered the main ozone depleting substance currently emitted, and no reduction is expected in the remaining years of the century. The significance of the impact on the stratosphere consists of the tendency of N<sub>2</sub>O to react with atomic oxygen, becoming the major natural source of NO<sub>x</sub>, identified as the largest contributor of ozone loss [1]. The primary N<sub>2</sub>O sources comprise the production of adipic and nitric acid, responsible for producing gaseous streams containing 20–50 vol% and 0.03–0.35 vol% of N<sub>2</sub>O, respectively [2]. As the atmospheric concentration of N<sub>2</sub>O continues to grow, it could double by 2050 [3]. In this context, the development of effective solutions to reduce the N<sub>2</sub>O emissions is becoming increasingly urgent. Among several N<sub>2</sub>O abatement technologies, the catalytic decomposition process is the most promising due to its cost-effectiveness and simplicity [4]. The N<sub>2</sub>O decomposition is an exothermic irreversible reaction (1), thus thermodynamic limitations are present. However, the choice of the catalyst is essential to efficiently obtain the breakage of the N–O bond in the N<sub>2</sub>O molecule [5], as seen in Equation (1):



The  $N_2O$  catalytic decomposition generally occurs in the temperature range 350–500 °C, depending on the catalytic species employed [6–9], requiring a certain amount of thermal energy. To this end, nowadays, most of the industrial processes produce thermal energy for the reaction by burning fossil fuels and providing the heat to the catalytic zone from the external side of the reactor. In this case, a decreasing temperature profile is obtained (red curve in Figure 1), since higher temperatures are needed outside the reactor to reach the reaction temperature in the middle of the catalytic bed. As a result, greenhouse gas emissions, high heat transfer resistance, and energy losses are obtained (Figure 1). In this context, microwave-assisted catalytic reactions have attracted great interest from the scientific sphere due to the advantages related to the microwave heating phenomena [10–13]. Microwave (MW) radiation can selectively heat certain materials rather than others based only on the dielectric properties of the sample [14,15]. This feature results in being very interesting for heterogeneous catalysis and for those processes where a certain amount of thermal energy is required. Microwave heating technology allows for the achievement of volumetric and selective heating of the catalytic bed. The heat flux is directed from the inside to the outside of the catalytic bed (blue curve in Figure 1), therefore, it is inverted with respect to the conventional heating, leading to a minimization of the energy losses and a more uniform temperature profile inside the catalytic bed. Consequently, better catalytic performance and a lower processing time may be obtained [16]. Furthermore, the microwave heating is an electricity-based technology, thus it finds room in the path towards the electrification of the industrial processes, assuring more environmental sustainability [17].

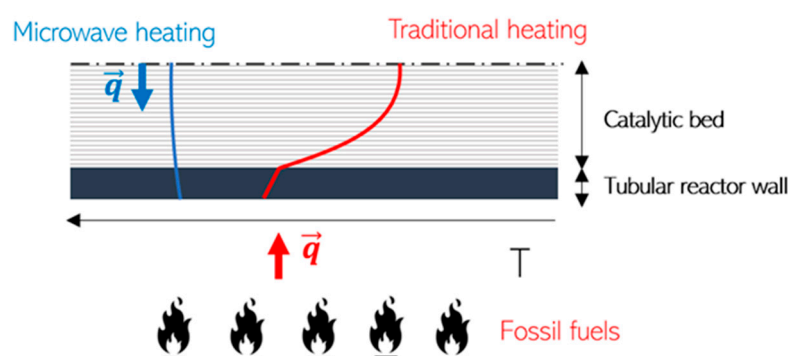


**Figure 1.** Comparison of temperature radial profile with traditional and microwave heating techniques.

Although several studies started few decades ago, the progress of the research in the field of microwave-assisted chemical catalytic processes is still at an early stage. In the present literature, the reported experimental studies involve different chemical reactions, such as the methane steam and dry reforming [16,18], dehydrogenation of alkanes into alkenes [19–24], and biomass pyrolysis [25,26]. Although the advantages of microwave heating technology as an alternative to the conventional one have been experimentally demonstrated, a commercial-scale plant is not yet present, especially due to the complexity of the system. In MW-assisted catalytic systems, particularly in heterogeneous catalysis, the key factor is the dielectric properties of the catalytic bed which must be a good microwave absorbing media. The most critical challenge is finding materials with both high microwave heating capacity and good catalytic performance for the reaction at issue. Among several materials, silicon carbide (SiC) is characterized by excellent microwave heating capability that can be measured considering different factors, such as the penetration depth of microwaves into the material, as shown in Table 1 [27]. As well as heating up rapidly and easily, SiC possesses many other excellent properties such as high fracture strength, high thermal conductivity, low chemical reactivity, high oxidation resistance, and wear resistance [28]. Thanks to these characteristics, SiC monoliths are ideal microwave-susceptible structured supports in catalytic reactions. The activation of the bare SiC monoliths generally consists of an alumina-based washcoat deposition that assures good adhesion of the species to the monolith's surface [29].

**Table 1.** Penetration depth (Dp) of microwaves (2.45 GHz) into some selected materials at 25 °C [27].

Material	Dp ( $\mu\text{m}$ )	Microwave Heating Capability
Fe <sub>2</sub> O <sub>3</sub>	$10 \times 10^6$	Transparent
	$<45 \times 10^3$ (600 °C)	Good
Al <sub>2</sub> O <sub>3</sub>	$12.6 \times 10^6$	Transparent
	$4.65 \times 10^6$ (590 °C)	Transparent
	$0.84 \times 10^6$ (980 °C)	Poor
	$0.18 \times 10^6$ (1340 °C)	Poor
Water	$3 \times 10^4$	Good
Fe <sub>3</sub> O <sub>4</sub>	80	Very good
SiC	$1.93 \times 10^6$	Excellent
Graphite (20–80 $\mu\text{m}$ )	$1.34 - 2.09 \times 10^4$	Excellent
Mg	2.2	For bulk metals: poor
Cu	2.7	For fine particles: good
Fe	1.3	
Ni	2.5	
Al	1.7	
Au	1.5	

The catalytic decomposition of nitrous oxide has been widely studied and it has been found that the transition metal oxides are the most active species, especially cobalt-based mixed oxides [30–35]. In our previous work [36], a SiC-based structured catalyst was investigated for the catalytic decomposition of nitrous oxide. The results demonstrated that a catalytic system as performant as the powders can be successfully achieved by depositing a nickel–cobalt–aluminum mixed oxide over a SiC honeycomb monolith. The advantages of using structured catalysts are not only related to the compactness of the configuration, but also to the reduced pressure drop and the better mass and heat transfer inside the catalytic zone, resulting in very promising systems [37]. Based on the interesting results obtained, and due to the microwave susceptibility of the SiC material, a further study has been carried out with the aim of investigating the performance of the SiC-based structured catalyst with the microwave heating technology for the decomposition of N<sub>2</sub>O. To the best of our knowledge, no studies on this topic are currently available in scientific literature.

In particular, in the present work, two different alumina-modified nickel–cobalt-based structured samples were prepared and characterized. The most promising formulation was transferred over SiC structures, and the N<sub>2</sub>O decomposition reaction was conducted with both microwave and traditional heating technologies, in order to compare the systems and investigate the advantages of the innovative process. Regarding the N<sub>2</sub>O concentration present in the gaseous stream subjected to the catalytic decomposition process, the experimental activities reported in the current literature were conducted by treating up to 2 vol% N<sub>2</sub>O. In the present work, high concentrations of N<sub>2</sub>O in inert stream have been studied, specifically from 20 vol% to 50 vol% N<sub>2</sub>O, to resemble a typical composition of downstream currents from adipic acid production plants.

## 2. Materials and Methods

### 2.1. Catalysts Preparation and Characterization

In this work, the structured catalysts were prepared by using SiC honeycomb monoliths (flow-through configuration, with all the channels open) due to the excellent microwave heating capability. The preliminary phase of the study was dedicated to the preparation of two different structured samples. Prior to each preparation, all the SiC monoliths were pretreated in air at 1000 °C for 48 h to obtain a layer of SiO<sub>2</sub> on the carrier surface that furthers the washcoat adherence [16].

The first sample, namely NiCo/Al<sub>2</sub>O<sub>3</sub>/SiC(0), was obtained by dispersing a nickel–cobalt mixed oxide into an alumina washcoat and depositing the obtained slurry over

the SiC carrier (size:  $37 \times 22 \times 10$  mm) via dip-coating procedure. The whole sample preparation can be summarized as follows:

- i. The nickel–cobalt mixed oxide was prepared through the co-precipitation method. Cobalt nitrate hexahydrate and nickel nitrate hexahydrate precursor salts were dissolved in water (about 7 mL of water was used for g of solid). The solution was stirred at room temperature for 5 min. Then,  $\text{NH}_{3,\text{aq}}$  (32 wt%) was added to the solution until the pH reached 9 to obtain the precipitation. After the filtration of the resultant precipitate with a filter paper, the filtrate was washed, dried at  $120^\circ\text{C}$  overnight, and calcinated in air at  $600^\circ\text{C}$  for 3 h ( $10^\circ\text{C}/\text{min}$  heating rate). The amount of precursor salts was chosen based on a Ni:Co value equal to 0.3, according to the literature [31].
- ii. The preparation of the alumina-based washcoat was carried out starting from an aqueous solution composed as follows: 80 wt% consists of distilled water and methylcellulose (1 wt% with respect to the water), and the remaining 20 wt% is composed by pseudoboehmite (10 wt%) with the addition of the nickel–cobalt mixed oxide powder that was previously achieved. The resultant washcoat slurry was kept under stirring for 24 h.
- iii. The  $\text{NiCo}/\text{Al}_2\text{O}_3/\text{SiC}(0)$  sample was obtained by means of dip-coating repeated cycles of the SiC monolith in the same slurry until reaching 10 wt% of deposited species with respect to the bare monolith. Drying at  $120^\circ\text{C}$  and calcination in air at  $600^\circ\text{C}$  for 3 h were performed between cycles.

The second sample,  $\text{NiCoAl}/\text{SiC}(0)$ , was achieved by depositing a nickel–cobalt–aluminum mixed oxide on the SiC monolith. The difference with the previous formulation lays in the formation of a trimetallic oxide where the aluminum is inside the metal lattice, while the previous formulation was characterized by a solid mixture of nickel–cobalt oxide and alumina. Cobalt nitrate hexahydrate, nickel nitrate hexahydrate, and aluminum nitrate hexahydrate were added to water (the same amount of water previously specified was used). Afterwards, the solution was stirred at room temperature for 5 min,  $\text{NH}_{3,\text{aq}}$  (32 wt%) was used as basifying substance to induce the co-precipitation. Instead of separating the precipitate, in this case, the resultant slurry was stirred for 24 h. Then, the slurry was employed for the dip-coating procedure, obtaining the sample  $\text{NiCoAl}/\text{SiC}(0)$ .

$\text{NiCo}/\text{Al}_2\text{O}_3/\text{SiC}(0)$  and  $\text{NiCoAl}/\text{SiC}(0)$  samples are shown in Figure 2, where they seem to be similar. More detailed images were obtained through a  $40\times$  optic microscope objective (Figure 3), to qualitatively appreciate the strong difference between the samples.

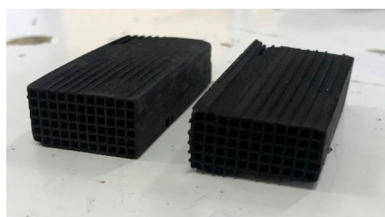


**Figure 2.**  $\text{NiCo}/\text{Al}_2\text{O}_3/\text{SiC}(0)$  (on the left) and  $\text{NiCoAl}/\text{SiC}(0)$  (on the right) samples prepared for the preliminary study.

After a preliminary study, as the  $\text{NiCoAl}/\text{SiC}(0)$  sample was more promising for the process under investigation, two final structured catalysts, namely  $\text{NiCoAl}/\text{SiC}(A)$  and  $\text{NiCoAl}/\text{SiC}(B)$ , were prepared. For these samples, the same formulation of  $\text{NiCoAl}/\text{SiC}(0)$  was maintained, but they were shaped differently, according to the diameter of the reactors employed for the catalytic activity tests in case of conventional and microwave heating, respectively (Figure 4).  $\text{NiCoAl}/\text{SiC}(A)$  catalyst is 7 cm long, has a square section of  $1.3\text{ cm} \times 1.3\text{ cm}$ , and 49 channels, while  $\text{NiCoAl}/\text{SiC}(B)$  is characterized by a length of 12 cm, a square section corresponding to  $3.1\text{ cm} \times 3.1\text{ cm}$ , and 196 channels.

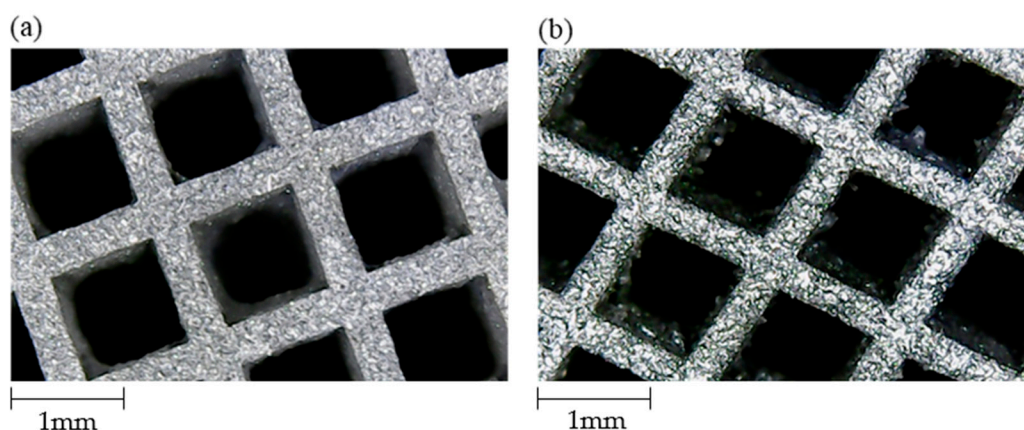


**Figure 3.** Images of NiCo/Al<sub>2</sub>O<sub>3</sub>/SiC(0) (a) and NiCoAl/SiC(0) (b) samples obtained through a 40X optic microscope objective.

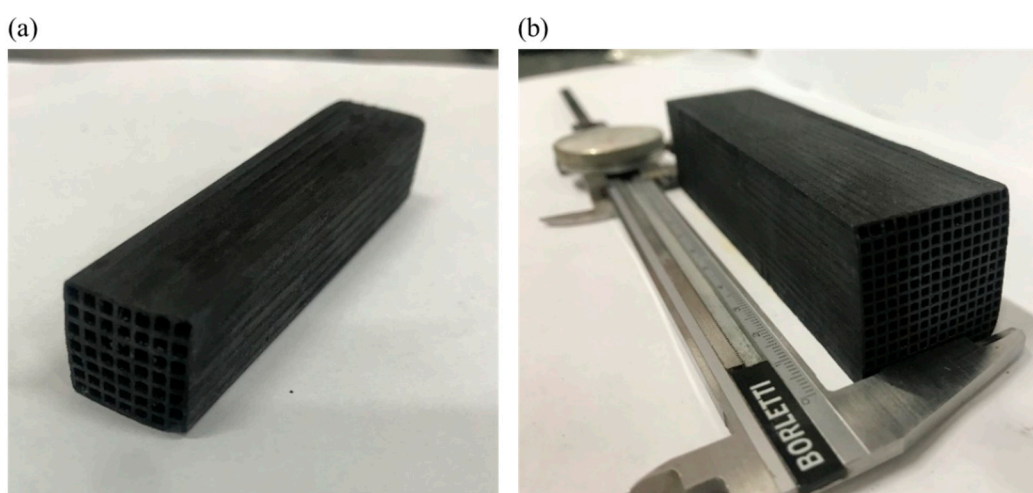


**Figure 4.** Images of NiCoAl/SiC(A) (a) and NiCoAl/SiC(B) (b) samples prepared for catalytic activity tests with conventional and microwave heating systems, respectively.

The catalysts were characterized by means of several techniques. The SEM/EDX analysis was performed through a Scanning Electron Microscope Mod.XL30 that is coupled to an Energy Dispersive X-ray Spectrometer (Philips, Oxford). The specific surface area was determined by means of N<sub>2</sub> adsorption at 196 °C applying BET method in NOVA-touch sorptometer. The evaluation of the washcoat mechanical resistance was carried out through repeated cycles of ultrasound adherence test by using an ultrasonic bath where the structured samples were stressed for 5 min at room temperature (60% of power with respect to the maximum was used). The porosimetric features of the catalysts before and after the active species deposition were obtained by means of the Hg penetration technique, with “PASCAL 140” and “PASCAL 240” instruments (Thermo Finnigan Instruments). The reducibility of the catalyst was investigated through H<sub>2</sub>-TPR, loading the sample NiCoAl/SiC(A) in a stainless-steel tubular reactor coupled to a Hiden Analytical mass spectrometer for the analysis. The test was performed in the temperature range 20–600 °C in the presence of a reducing mixture 5 vol% H<sub>2</sub>-Ar and with a heating rate of 10 °C/min. Other characterization techniques have been previously used and the details were given in a previous work [36].

## 2.2. Laboratory Apparatus and Procedure

The catalytic activity of the structured samples during the decomposition of N<sub>2</sub>O was investigated in both conventional and microwave heating systems, thus two different

experimental apparatus were employed. In the first case, the NiCoAl/SiC(A) structured sample was placed in a fixed bed reactor (AISI 310 stainless steel, 17 mm internal diameter, 320 mm long). The heat to the reaction section was supplied by means of an electrical furnace where the reactor was in horizontal position. Further details about the experimental apparatus used for the conventional heating mode tests can be found in our previous work [36]. The microwave-assisted  $N_2O$  decomposition reaction was studied in a laboratory plant that differs essentially from the heat providing system and the reactor configuration. The microwave apparatus consists of: (i) a power generator, equipped with an external analog signal controller that can adjust the output power up to 2 kW; (ii) a magnetron coupled with a cooling fan to avoid overheating phenomena; and (iii) a waveguide and a microwave cavity that corresponds to the reactor itself. The reactor geometry is essential to reach optimal heating of the catalytic zone. In this regard, the experimental tests were performed in a peculiar reactor configuration [38] characterized by a restriction in correspondence of the catalytic section as shown in Figure 5. The cone-shaped geometry at the inlet and the outlet can intensify the electric field of microwaves in the catalytic zone, minimizing reflected radiation phenomena. Furthermore, the reactor is equipped with an air chamber that surrounds the internal wall of the reactor in order to obtain thermal integration. In addition to assuring thermal insulation, this configuration guarantees the preheating of the incoming gas that passes through the chamber and enters the reactor cavity from three holes placed below at  $120^\circ$  apart.

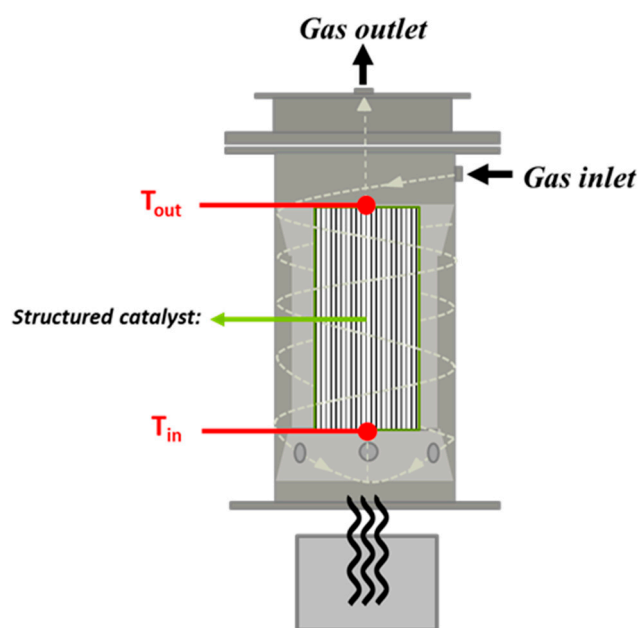


**Figure 5.** Reactor configuration used for the microwave-assisted  $N_2O$  decomposition tests.

In Figure 6, a scheme of the experimental apparatus is illustrated. The gaseous stream passes through RESTEK moisture traps to ensure completely anhydrous feeding to the reaction section. A battery of Bronkhorst mass flow controllers was used to adjust the gas composition and a valves system allows for the selection of the reaction mode or the bypass mode to send the gaseous mixture to the reactor or to the analysis system, respectively. The structured catalyst is placed in the reactor in a quartz wool layer to assure a good adhesion to the walls and a lower heating dissipation towards the external environment. Since the application of conventional metal thermocouples may not provide an accurate measurement, fiber optic sensors (Optocon TS2) were employed to detect the temperature at the inlet and the outlet of the catalytic zone. The gaseous mixture was analyzed by means of a mass spectrometer (Pfeiffer Vacuum OmniStar) coupled with QUADSTAR 422 software.

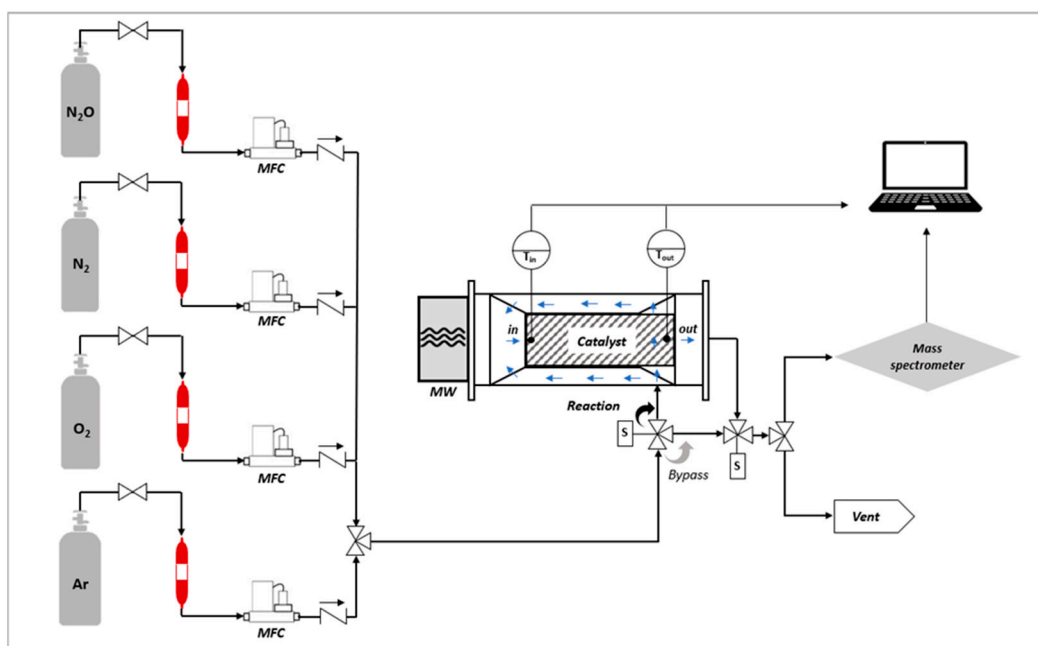


Figure 6. Scheme of the microwave experimental plant.

The  $\text{N}_2\text{O}$  decomposition reaction was investigated over the structured catalysts in a temperature range of 200–600 °C, at three weight hourly space velocity (WHSV) values, i.e.,  $2.5 \text{ h}^{-1}$ ,  $5 \text{ h}^{-1}$ , and  $20 \text{ h}^{-1}$ , which refer to the catalyst mass deposited on the structured carrier as described in the Equation (2), where  $\dot{W}$  indicates the total mass flow rate. In the microwave-assisted experimental tests, the desired temperature in the catalytic zone was obtained by adjusting the MW generator power from 400 W to 800 W. Moreover, the reactants stream and the microwaves were sent to the reactor in co-current mode, thus the gaseous stream entered the reactor from the most irradiated catalytic zone. In order to observe the effect of  $\text{N}_2\text{O}$  concentration on the catalytic performance, experimental tests were conducted by feeding gaseous mixtures with different compositions, namely 20 vol% and 50 vol% of  $\text{N}_2\text{O}$  in argon as inert gas. Before each test, the reaction environment was pretreated for 1 h at 600 °C by sending an argon stream containing 5 vol% of  $\text{O}_2$ . The performance of the system was monitored by observing the  $\text{N}_2\text{O}$  conversion trends. Regarding the selectivity towards the desired reaction, NO and  $\text{NO}_2$  subproducts formation has been controlled.

$$\text{WHSV} = \frac{\dot{W}}{m_{\text{cat}}} \quad (2)$$

### 3. Results and Discussion

#### 3.1. Catalysts Characterization

In the preparation of a structured catalyst, the adherence of the deposited species is a key parameter, since it can determine the lifetime of the catalyst; furthermore, the ease of the preparation, in terms of number of cycles necessary to reach the desired loading, can also be determining. Both these aspects are reported in Figure 7.

The adherence of the coating deposited onto the  $\text{NiCoAl}/\text{SiC}(0)$  and  $\text{NiCo}/\text{Al}_2\text{O}_3/\text{SiC}(0)$  samples was evaluated by measuring the weight loss resulting from the ultrasound stress to which the samples were subjected. The samples were dipped in a beaker filled with petroleum ether [39] and treated through repeated cycles of 5 minutes in an ultrasound bath until there was no change in weight variation between two consecutive cycles. Figure 7a illustrates the percentage weight loss obtained after each cycle, and the results highlight the better adherence of the coating deposited on the  $\text{NiCoAl}/\text{SiC}(0)$  sample with respect to the  $\text{NiCo}/\text{Al}_2\text{O}_3/\text{SiC}(0)$ ; indeed, the weight loss detected after 5 ultrasound cycles in

the case of NiCoAl/SiC(0) is only 2.9% against 8.2% obtained with NiCo/Al<sub>2</sub>O<sub>3</sub>/SiC(0). The difference in mechanical stability of the coating can be ascribed to the distinct chemical nature of the two slurry formulations. Specifically, in the case of NiCo/Al<sub>2</sub>O<sub>3</sub>/SiC(0), the deposited species consist of a mix of oxides (alumina and Ni–Co mixed oxide), while the NiCoAl/SiC(0) is characterized by the presence of a Ni–Co–Al mixed oxide. The evidence of the differences in the chemical nature of these compounds was deeply described in the previous work [36] after the study of several powder catalyst formulations for the N<sub>2</sub>O decomposition reaction. Figure 7b shows that three and four cycles were necessary to prepare NiCo/Al<sub>2</sub>O<sub>3</sub>/SiC(0) and NiCoAl/SiC(0), respectively, suggesting that the higher stability of the latter could also be attributed to the more gradual deposition of the active phase.

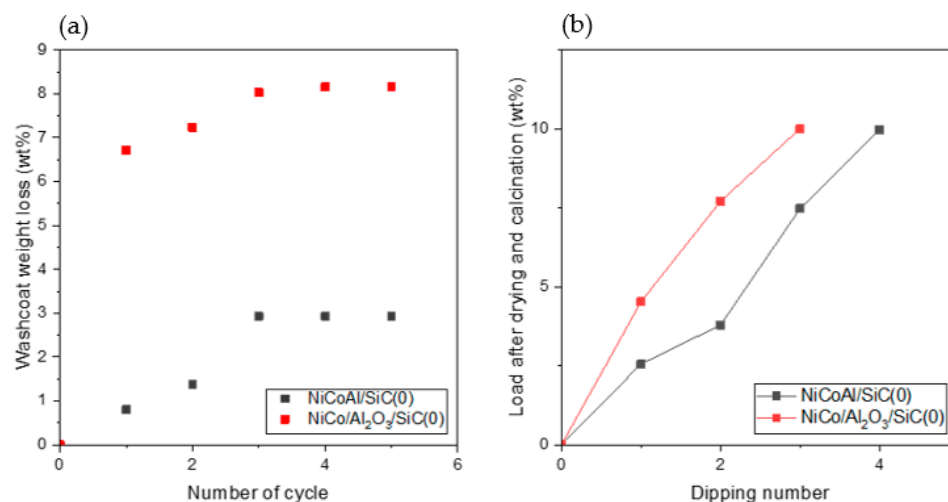


**Figure 7.** Ultrasound adherence test (a) and active phase loading evolution after drying and calcination (b).

Even though the role of the structured catalysts mechanical resistance is essential in the choice of the most suitable washcoat formulation, the textural properties also play a crucial role in the catalytic behavior. The samples NiCoAl/SiC(0) and NiCo/Al<sub>2</sub>O<sub>3</sub>/SiC(0) were characterized by means of Hg penetration technique. The comparison of the grey and red continuous curves representing the pore size distribution, as well as the evolution of the Hg intruder volume in Figure 8a indicate the presence of pores smaller than 1  $\mu\text{m}$  in NiCo/Al<sub>2</sub>O<sub>3</sub>/SiC(0) compared to NiCoAl/SiC. Specifically, in the case of NiCoAl/SiC(0), the average and median pore diameters are equal to 15.6  $\mu\text{m}$  and 17.5  $\mu\text{m}$ , respectively, against the 2.6  $\mu\text{m}$  and 14.6  $\mu\text{m}$  of NiCo/Al<sub>2</sub>O<sub>3</sub>/SiC(0). A more comprehensive view about the textural characteristics of the samples was obtained by means of the physisorption of N<sub>2</sub> at  $-196\text{ }^\circ\text{C}$ , a technique that can also detect the presence of mesopores. The results summarized in Table 2 showed that the transfer of the Ni–Co–Al mixed oxide onto the SiC monolith leads to higher SSA of NiCoAl/SiC(0) with respect to the NiCo/Al<sub>2</sub>O<sub>3</sub>/SiC(0) sample. The isotherm curves reported in Figure 8b can be ascribed to type IV isotherm, according to 1985 IUPAC recommendations [40], but are characterized by two different hysteresis. This last result may indicate the presence of pores with different structures. In any case, the higher adsorbed volume of the grey curve, relevant to NiCoAl/SiC(0), indicated the presence of a higher pore volume with respect to the other sample, as reported in Table 2. All these results seem to suggest a worst dispersion of the active phases on the NiCo/Al<sub>2</sub>O<sub>3</sub>/SiC(0) sample. Effectively, during the preparation phase of the two structured samples, as shown in Figure 7b, the final load was obtained more gradually in the NiCoAl/SiC(0) sample with respect to the NiCo/Al<sub>2</sub>O<sub>3</sub>/SiC(0) sample. It depends on the chemical nature of the distinct slurries employed that visibly exhibited different viscosities. In this regard, it is reported that the washcoat load is affected by the rheological behavior [41]. Specifically, for each dipping cycle, lower loads were deposited in the case of NiCoAl/SiC(0), whose slurry was characterized by lower viscosity, according to

literature. As a consequence, in order to reach the same percentage of washcoat loads, the NiCoAl/SiC(0) sample needed one more dipping cycle, evidently assuring better dispersion of the active phase.

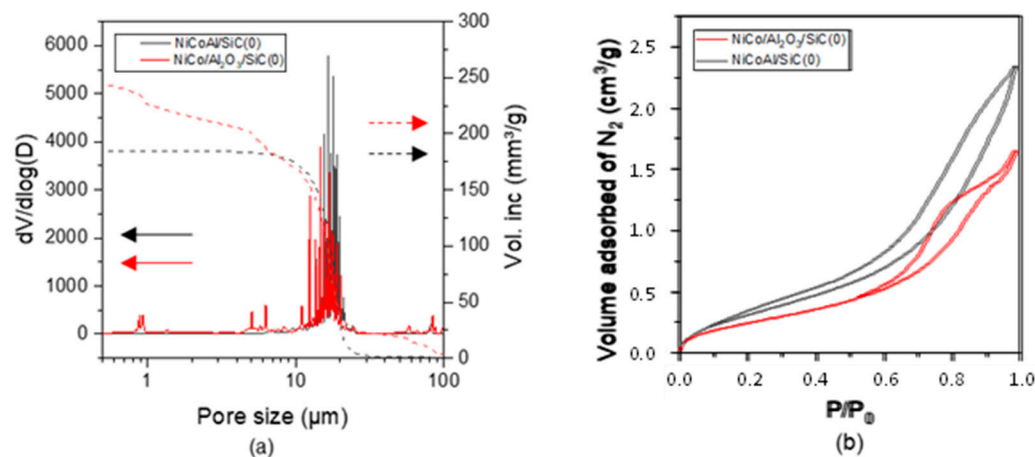


**Figure 8.** Pore size distribution and evolution of the intruder Hg volume (a) and N<sub>2</sub> adsorption-desorption isotherm curves (b): comparison between the NiCoAl/SiC(0) and NiCo/Al<sub>2</sub>O<sub>3</sub>/SiC(0) samples.

**Table 2.** Specific surface area, pore volume, and pore radius average measurement obtained through adsorption of N<sub>2</sub> at −196 °C.

Sample	SSA (B.E.T.) (m <sup>2</sup> /g)	Pore Volume (cm <sup>3</sup> /g)	Pore Radius (nm)
NiCoAl/SiC(0)	1.34	0.004	2.27
NiCo/Al <sub>2</sub> O <sub>3</sub> /SiC(0)	0.99	0.002	1.53

The NiCoAl/SiC(0) sample was further characterized by means of SEM/EDX analysis. Figure 9 illustrates the electronic image of the sample (a) that shows the surface morphology of the catalytic layer deposited on the SiC monolith, as well as the EDX stratified and single images of the different deposited species (b,c), highlighting a homogeneously dispersed catalyst over the SiC carrier.

As a consequence of the results of all the characterization techniques, the final structured samples for the catalytic experimental activity tests were prepared by choosing the NiCoAl/SiC(0) formulation. In fact, the results discussed in this paragraph suggest that NiCoAl/SiC(0) is characterized by higher mechanical stability, higher specific surface area, and better dispersion of the active phase on the SiC structure which can lead to the most promising catalytic behavior. Furthermore, in our previous work [36], the N<sub>2</sub>O decomposition reaction investigated on powder catalysts with similar chemical formulations resulted in better catalytic performance of Ni–Co–Al-based mixed oxide with respect to Ni–Co-based oxide over alumina. On the basis of the above considerations, the NiCoAl/SiC(0) sample was selected as the most promising structured catalyst, thus, it was reproduced in two final specific sizes, namely NiCoAl/SiC(A) and NiCoAl/SiC(B).

The N<sub>2</sub>O decomposition reaction mechanism involves the production of oxygen atoms adsorbed on the catalyst that form O<sub>2</sub> and desorb [42]. As a result, the reducibility of the catalytic species is highly relevant for the process at issue. The H<sub>2</sub>-TPR profile recorded for the NiCoAl/SiC(0) catalyst is displayed in Figure 10. The results show a H<sub>2</sub> consumption peak at 250–550 °C, ascribable to the reduction of NiO and CoO to metallic form [43]. Therefore, the reduction of the species at relatively low temperatures is indicative of good catalytic activity.

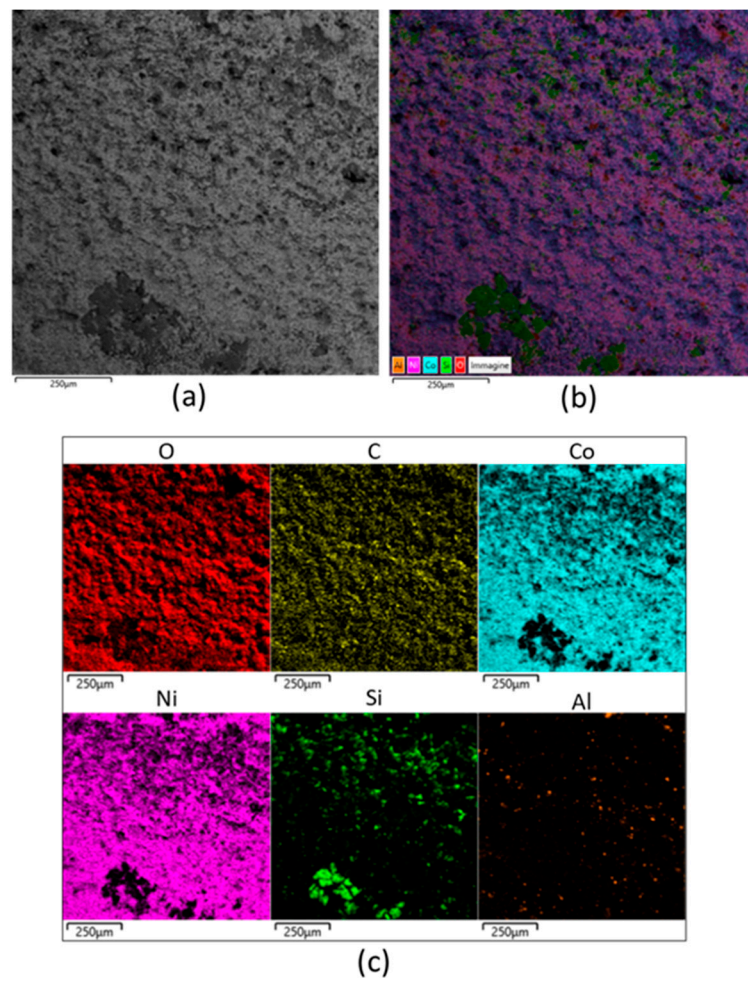


**Figure 9.** SEM/EDX images of the NiCoAl/SiC(0) sample. (a,b): reference image; (c): element mapping.

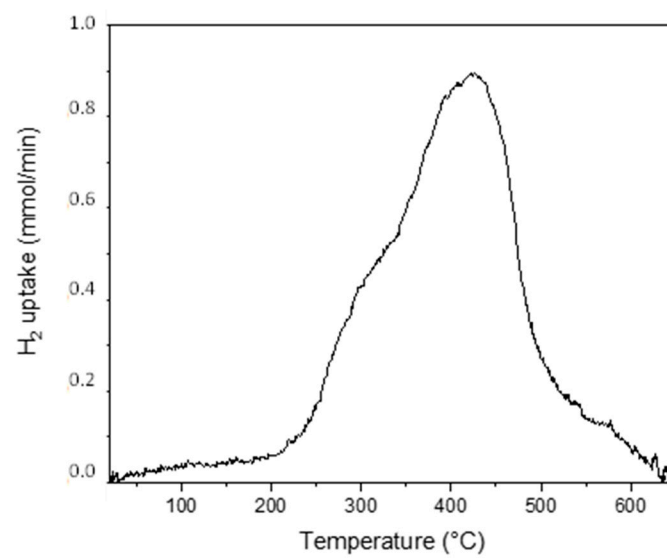


**Figure 10.** H<sub>2</sub>-TPR over the NiCoAl/SiC(0) sample.

### 3.2. Experimental Tests

#### 3.2.1. Preliminary Microwave Heating Test

It is well-known that the temperature profile inside the catalytic volume notably affects the performance of the system. Therefore, a preliminary microwave heating test on a SiC bare monolith was carried out with the aim of observing the thermal effect of the microwave radiation by keeping the generator power unchanged (300 W). Specifically, the test was conducted in an Ar stream (1000 NmL/min) by using the appropriate reactor configuration already described before. The monolith inlet and outlet temperatures were detected during the microwave heating until constant values were reached. The results of the test, reported in Figure 11, show that the warmer zone of the monolith corresponds to the inlet, according to the direction of the microwave radiation. The gap between the temperatures decreased with time: the inlet was rapidly heated by the effective microwaves' interaction with the monolith, while in the remaining zone, further from the microwave source, the radiation effect was reduced with respect to the inlet, thus the excellent conductive property of the SiC heated the whole monolith. The axial temperature profile obtained with the microwave heating method in inert environment conditions is expected to change by the effect of the exothermicity of the  $N_2O$  decomposition reaction, and as discussed in the following paragraph, it occurs differently from the case of traditional heating. A further aspect to consider is that the heating of the catalytic zone up to 500 °C was reached in a time of 30 min, confirming the rapid and easy microwave heating technique.

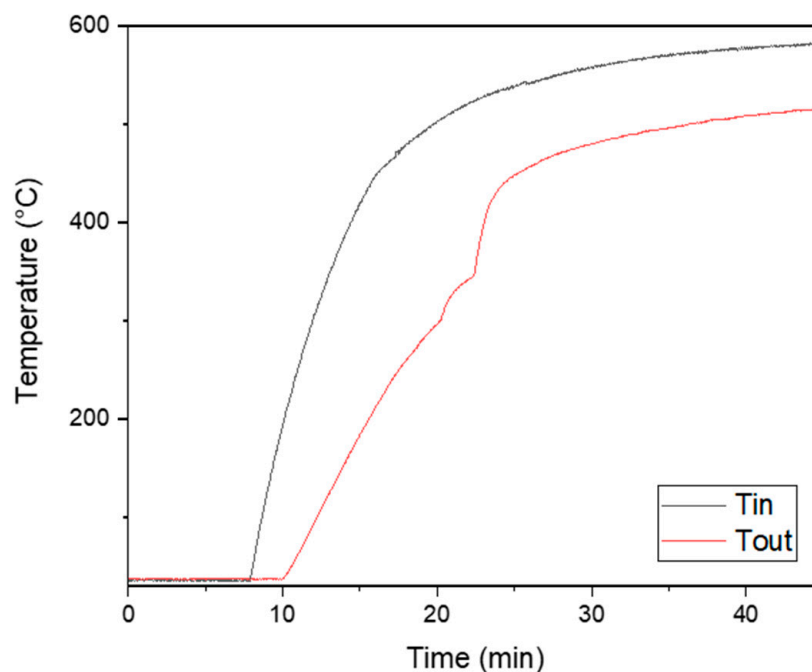
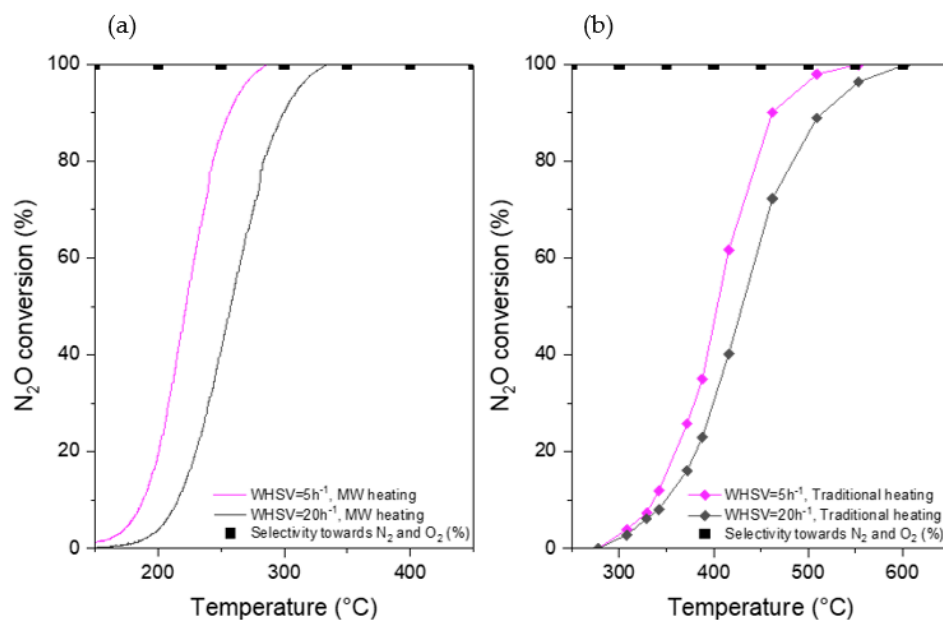


Figure 11. MW heating test on bare SiC monolith.

#### 3.2.2. Catalytic Activity Tests

The catalytic decomposition of  $N_2O$  was performed by using both traditional and microwave heating technologies over the structured catalysts NiCoAl/SiC(A) and NiCoAl/SiC(B), respectively, in order to compare the results and appreciate the differences between the systems. As previously described, the two structured catalysts mentioned above only differ in size, that were opportunely selected for the reactor geometry, and in order to conduct the activity tests in the same WHSV operative conditions, making comparable the two different systems. The first set of experiments were conducted by treating a gaseous mixture containing 20 vol%  $N_2O$  in Ar stream at two different space velocity (WHSV) values of  $5 h^{-1}$  and  $20 h^{-1}$ . In Figure 12, the results of the catalytic performance in different operative conditions were illustrated in terms of  $N_2O$  conversion. The comparison between

the results obtained from traditional and microwave heating technology raises important considerations. The microwave heating technology led to an improvement of the system performance: by keeping the space velocity values unchanged, total  $N_2O$  conversion was achieved at considerably lower temperatures with respect to the traditional heating. Specifically, at  $20\text{ h}^{-1}$  and  $5\text{ h}^{-1}$ , 100% of  $N_2O$  conversion was reached at  $420\text{ }^\circ\text{C}$  and  $340\text{ }^\circ\text{C}$ , respectively, in the case of MW heating, in contrast to  $600\text{ }^\circ\text{C}$  and  $510\text{ }^\circ\text{C}$  in the case of traditional heating. In both systems, as expected, by increasing the contact time, the conversion curves shift towards lower temperatures. The thermal profile obtained inside the catalytic bed may explain the excellent performance assured by the microwave heating technique: during the activity test conducted with the conventional heating mode, the heat flux provided from the external side of the reactor homogeneously heats the catalytic zone, also due to the high thermal conductivity of the SiC monolith. However, the exothermicity of the  $N_2O$  decomposition reaction tends to form a growing axial temperature profile along the structured catalyst; on the contrary, due to the magnetron purposely located at the catalyst inlet, the microwave heating mode, in absence of the reaction, allows for a decreasing axial profile to be obtained, as illustrated in the previous paragraph, that flattens during the chemical reaction due to the balancing effect of its exothermicity. The flatter temperature profile obtained by directly providing the heat to the monolith means the catalytic bed is more effectively exploited since most part of it works at higher temperatures with respect to the conventional heating configuration (Figure 13). In addition to the efficiency of the heating method, it is important to highlight the good performance of the catalytic system that, even under conventional heating conditions, successfully treats gaseous streams containing high concentrations of  $N_2O$ . Thus, the catalytic system can not only totally convert high concentrations of  $N_2O$  with a more compact configuration than the powder catalysts, but also perform the conversion at low temperatures by coupling the system to an alternative heating method.



**Figure 12.**  $N_2O$  decomposition reaction of the NiCoAl/SiC(A) and NiCoAl/SiC(B) catalysts by using traditional and MW heating technologies, respectively on (a) and (b) (20 vol%  $N_2O$  in Ar, 1 atm).

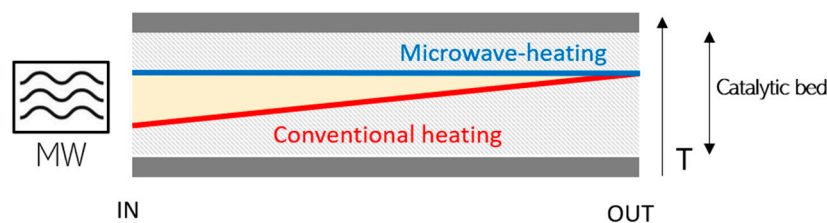


**Figure 13.** Illustration of thermal axial profile obtained during the  $\text{N}_2\text{O}$  decomposition reaction by means of conventional and microwave heating methods.

The catalytic activity was further investigated at higher  $\text{N}_2\text{O}$  concentration conditions, keeping the space velocity unchanged. Specifically, the microwave-assisted  $\text{N}_2\text{O}$  decomposition reaction was conducted over the NiCoAl/SiC(B) structured catalyst by sending a gaseous mixture containing 50 vol%  $\text{N}_2\text{O}$  in Ar stream at a WHSV value of  $5 \text{ h}^{-1}$ . As shown in Figure 14, by passing from 20 vol% to 50 vol%  $\text{N}_2\text{O}$ , the  $\text{N}_2\text{O}$  conversion curve shifted towards higher temperatures. Thus, greatly increasing the reactant concentration could change the reaction rate kinetic. According to the reaction mechanism reported in Ref. [42], the  $\text{N}_2\text{O}$  molecule reacts with an active site producing molecular  $\text{N}_2$  and obtaining an activated atomic oxygen ( $\text{O}^*$ ) whose combination with another ( $\text{O}^*$ ) generates  $\text{O}_2$ , with the release of two active sites, according to the Langmuir–Hinshelwood mechanism. It is clear that the higher the  $\text{N}_2\text{O}$  concentration, the lower the number of available active sites, consequently limiting the decomposition reaction. Despite the lower conversion at the same temperature, the results demonstrated that the microwave-assisted decomposition over a structured catalyst totally converts 50 vol%  $\text{N}_2\text{O}$  towards  $\text{N}_2$  and  $\text{O}_2$  at  $550 \text{ }^\circ\text{C}$ . This result is an outstanding achievement: the microwave-assisted process totally removed  $\text{N}_2\text{O}$  from a  $\text{N}_2\text{O}$ -rich gaseous stream at the same temperature required to purify a  $\text{N}_2\text{O}$ -lean stream in the thermal process, being the  $\text{N}_2\text{O}$ -rich stream is concentrated more than double in the pollutant compared to the lean stream.

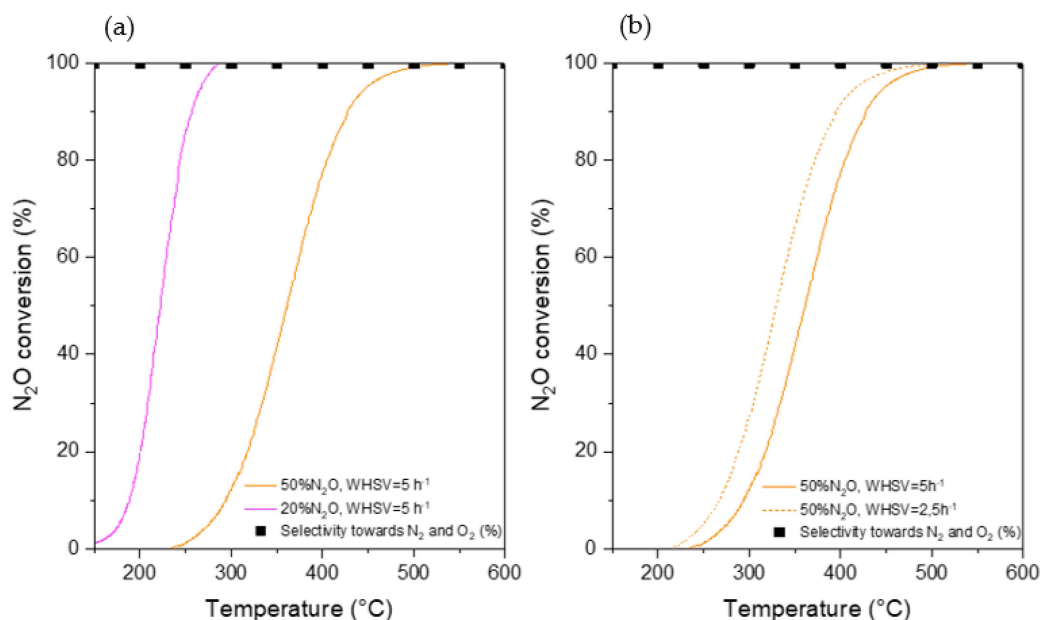


**Figure 14.** MW-assisted activity test over NiCoAl/SiC(B) at different operative conditions. (a) 50 vol% and 20 vol%  $\text{N}_2\text{O}$  at  $5 \text{ h}^{-1}$ ; (b) 50 vol%  $\text{N}_2\text{O}$  at 5 and  $2.5 \text{ h}^{-1}$ .

The same experimental activity test was conducted under a WHSV value of  $2.5 \text{ h}^{-1}$ , keeping the remaining operative conditions unchanged. The results in Figure 14 highlighted a shift of the  $\text{N}_2\text{O}$  conversion curve towards lower temperatures, even though the

temperature necessary to reach the total conversion was not particularly lower due to the small variation of the space velocity. Furthermore, it is important to notice that in all the activity experimental results, no NO and NO<sub>2</sub> by-product formation was detected, thus, the total selectivity of the system towards the desired products was achieved.

#### 4. Conclusions

In the framework of N<sub>2</sub>O removal from concentrated industrial streams, this study focused on the application of structured catalysts and microwave technology to this process. Through a preliminary evaluation, the suitability of deposition of different previously studied formulations was assessed. It was observed that the Ni–Co–Al trimetallic mixed oxide formulation (given as NiCoAl/SiC) was more promising both in terms of adherence and textural properties than the solid mixtures of alumina washcoat and Ni–Co mixed oxide (NiCo/Al<sub>2</sub>O<sub>3</sub>/SiC). Hence, the most suitable formulation was employed for the preparation of two structured catalysts to be applied in a conventional heating process and a microwave-assisted process. A complete screening of activity from 0% to total conversion was performed in different WHSV and N<sub>2</sub>O concentration conditions, revealing that the choice of lower WHSV decreases the temperature necessary to achieve the total conversion, while an increase in N<sub>2</sub>O concentration remarkably shifts the conversion curve to higher temperatures. In this context, it was proven that the application of microwave technology significantly lowers the energy demand of the process, thanks to the optimization of the temperature profile within the catalytic bed. As the outcome, the microwaves-assisted process is able to totally remove N<sub>2</sub>O from a highly concentrated stream (50 vol%) at 550 °C, which is the same temperature required in the conventionally heated process for the removal of N<sub>2</sub>O from a less concentrated gas stream (20 vol%).

**Author Contributions:** Conceptualization, O.M., E.M., S.R., M.M., F.B., P.P. and V.P.; methodology, O.M., E.M., S.R., M.M., F.B., P.P. and V.P.; software, O.M., E.M., S.R., M.M., F.B., P.P. and V.P.; validation, O.M., E.M., S.R., M.M., F.B., P.P. and V.P.; formal analysis, O.M., E.M., S.R., M.M., F.B., P.P. and V.P.; investigation, O.M., E.M., S.R., M.M., F.B., P.P. and V.P.; resources, O.M., E.M., S.R., M.M., F.B., P.P. and V.P.; data curation, O.M., E.M., S.R., M.M., F.B., P.P. and V.P.; writing—original draft preparation, O.M., E.M., S.R., M.M., F.B., P.P. and V.P.; writing—review and editing, O.M., E.M., S.R., M.M., F.B., P.P. and V.P.; visualization, O.M., E.M., S.R., M.M., F.B., P.P. and V.P.; supervision, O.M., E.M., S.R., M.M., F.B., P.P. and V.P.; project administration, O.M., E.M., S.R., M.M., F.B., P.P. and V.P.; funding acquisition, O.M., E.M., S.R., M.M., F.B., P.P. and V.P. All authors have read and agreed to the published version of the manuscript.

**Funding:** This research received no external funding.

**Data Availability Statement:** Not applicable.

**Acknowledgments:** The authors are grateful to Paolo Tramonti for performing the SEM-EDX analysis.

**Conflicts of Interest:** The authors declare no conflict of interest.

#### References

1. Stolarski, R.; Douglass, A.; Oman, L.; Waugh, D. Impact of future nitrous oxide and carbon dioxide emissions on the stratospheric ozone layer. *Environ. Res. Lett.* **2015**, *10*, 3. [[CrossRef](#)]
2. Miao, M.; Zhang, M.; Kong, H.; Zhou, T.; Yang, X.; Yang, H. Progress in Catalytic Decomposition and Removal of N<sub>2</sub>O in Fluidized Bed. *Energies* **2021**, *14*, 6148. [[CrossRef](#)]
3. Hu, X.; Wang, Y.; Wu, R.; Zhao, Y. N-doped Co<sub>3</sub>O<sub>4</sub> catalyst with a high efficiency for the catalytic decomposition of N<sub>2</sub>O. *Mol. Catal.* **2021**, *509*, 111656. [[CrossRef](#)]
4. Zhao, F.; Wang, D.; Li, X.; Yin, Y.; Wang, C.; Qiu, L.; Yu, J.; Chang, H. Enhancement of Cs on Co<sub>3</sub>O<sub>4</sub> for N<sub>2</sub>O catalytic decomposition: N<sub>2</sub>O activation and O<sub>2</sub> desorption. *Ind. Eng. Chem. Res.* **2022**, *61*, 13854–13862. [[CrossRef](#)]
5. Kapteijn, F.; Rodriguez-Mirasol, J.; Moulijn, J. Heterogeneous catalytic decomposition of nitrous oxide. *Appl. Catal. B Environ.* **1996**, *9*, 25–64. [[CrossRef](#)]
6. Bozorgi, B.; Karimi-Sabet, J.; Khadiv-Parsi, P. The removal of N<sub>2</sub>O from gas stream by catalytic decomposition over Pt-alkali metal/SiO<sub>2</sub>. *Environ. Technol. Innov.* **2022**, *26*, 102344. [[CrossRef](#)]
7. Zhao, T.; Gao, Q.; Liao, W.; Xu, X. Effect of Nd-incorporation and K-modification on catalytic performance of Co<sub>3</sub>O<sub>4</sub> for N<sub>2</sub>O decomposition. *J. Fuel. Chem. Technol.* **2019**, *47*, 1120–1128. [[CrossRef](#)]

8. Carabineiro, S.A.C.; Papista, E.; Marnellos, G.E.; Tavares, P.B.; Maldonado-Hódar, F.J.; Konsolakis, M. Catalytic decomposition of  $N_2O$  on inorganic oxides: Effect of doping with Au nanoparticle. *Mol. Catal.* **2017**, *436*, 78–89. [[CrossRef](#)]
9. Wang, J.; Xia, H.; Ju, X.; Fan, F.; Feng, Z.; Li, C. Catalytic performance of different types of iron zeolites in  $N_2O$  decomposition. *Chin. J. Catal.* **2013**, *34*, 876–888.
10. Chen, W.; Malhotra, A.; Yu, K.; Zheng, W.J.; Plaza-Gonzalez, P.; Catala-Civera, J.M.; Santamaria, J.; Vlachos, D.G.J. Intensified microwave-assisted heterogeneous catalytic reactors for sustainable chemical manufacturing. *Chem. Eng. J.* **2021**, *420*, 130476. [[CrossRef](#)]
11. Goyal, H. Process intensification using microwave heated multiphase reactors. *Chem. Eng. Process. Process Intensif.* **2022**, *178*, 109026. [[CrossRef](#)]
12. Kumar, A.; Kuang, Y.; Liang, Z.; Sun, X. Microwave chemistry, recent advancements, and eco-friendly microwave-assisted synthesis of nanoarchitectures and their applications: A review. *Mater. Today Nano* **2020**, *11*, 100076. [[CrossRef](#)]
13. Ricciardi, L.; Verboom, W.; Lange, J.; Huskens, J. Reactive Extraction Enhanced by Synergic Microwave Heating: Furfural Yield Boost in Biphasic Systems. *ChemSusChem* **2020**, *13*, 3589–3593. [[CrossRef](#)] [[PubMed](#)]
14. Muley, P.D.; Wang, Y.; Hu, J.; Shekhawat, D. Microwave-assisted heterogeneous catalysis. *Catalysis* **2021**, *33*, 460.
15. Palma, V.; Barba, D.; Cortese, M.; Martino, M.; Renda, S.; Meloni, E. Microwaves and Heterogeneous Catalysis: A Review on Selected Catalytic Processes. *Catalysts* **2020**, *10*, 246. [[CrossRef](#)]
16. Meloni, E.; Martino, M.; Ricca, A.; Palma, V. Ultracompact methane steam reforming reactor based on microwaves susceptible structured catalysts for distributed hydrogen production. *Int. J. Hydrogen Energy* **2021**, *46*, 13729–13747. [[CrossRef](#)]
17. Stankiewicz, A.; Sarabi, F.E.; Baubaid, A.; Yan, P.; Nigar, H. Perspectives of Microwaves-Enhanced Heterogeneous Catalytic Gas-Phase Processes in Flow Systems. *Chem. Rec.* **2019**, *19*, 40–50. [[CrossRef](#)]
18. De Dios, I.; Andrzej, G.; Nigar, S.H. Syngas production via microwave-assisted dry reforming of methane. *Catal. Today* **2021**, *362*, 72–80. [[CrossRef](#)]
19. Ma, Z.; Xua, W.; Wang, Q.; Zhou, Q.; Zhou, J. Highly effective microwave catalytic oxidative dehydrogenation of propane by  $CO_2$  over V-La-doped dendritic mesoporous silica-based microwave catalysts. *Chem. Eng. J.* **2022**, *435*, 135081. [[CrossRef](#)]
20. Eryildirim, B.; Arbag, H.; Oktar, N.; Dogu, G. Comparison of microwave and conventionally heated reactor performances in catalytic dehydrogenation of ethane. *Int. J. Hydrogen Energy* **2021**, *46*, 5296–5310. [[CrossRef](#)]
21. Wang, Q.; Xu, W.; Ma, Z.; Yu, F.; Chen, Y.; Liao, H.; Wang, X.; Zhou, J. Highly Effective Direct Dehydrogenation of Propane to Propylene by Microwave Catalysis at Low Temperature over CoSn/NC Microwave Catalyst. *ChemCatChem* **2021**, *13*, 1009–1022. [[CrossRef](#)]
22. Ramirez, A.; Hueso, J.L.; Mallad, R.; Santamaria, J. Microwave-activated structured reactors to maximize propylene selectivity in the oxidative dehydrogenation of propane. *Chem. Eng. J.* **2020**, *393*, 124746. [[CrossRef](#)]
23. Koyuncu, D.D.E. Microwave-assisted non-oxidative ethane dehydrogenation over different carbon materials. *Diam. Relat. Mater.* **2020**, *110*, 108130. [[CrossRef](#)]
24. Jie, X.; Xiao, T.; Yao, B.; Gonzalez-Cortes, S.; Wang, J.; Fang, Y.; Miller, N.; AlMegren, H.; Dilworth, J.R.; Edwards, P.P. On the performance optimisation of Fe catalysts in the microwave—assisted  $H_2$  production by the dehydrogenation of hexadecane. *Catal. Today* **2018**, *317*, 29–35. [[CrossRef](#)]
25. Mohamed, B.A.; Ellis, N.; Kim, C.S.; Bi, X. Microwave-assisted catalytic biomass pyrolysis: Effects of catalyst mixtures. *Appl. Catal. B Environ.* **2019**, *253*, 226–234. [[CrossRef](#)]
26. Gaudino, E.C.; Cravotto, G.; Manzoli, M.; Tabasso, S. From waste biomass to chemicals and energy via microwave-assisted processes. *Green Chem.* **2019**, *21*, 1202. [[CrossRef](#)]
27. Amini, A.; Latifi, M.; Chaouki, J. Electrification of materials processing via microwave irradiation: A review of mechanism and applications. *Appl. Therm. Eng.* **2021**, *193*, 117003. [[CrossRef](#)]
28. Julian, I.; Pedersen, C.M.; Achkasov, K.; Hueso, J.L.; Hellstern, H.L.; Silva, H.; Mallada, R.; Davis, Z.J.; Santamaria, J. Overcoming Stability Problems in Microwave-Assisted Heterogeneous Catalytic Processes Affected by Catalyst Coking. *Catalysts* **2019**, *9*, 867. [[CrossRef](#)]
29. Ruocco, C.; Coppola, A.; Picciotti, G.; Palma, V. Experimental study of the oxidative steam reforming of fuel grade bioethanol over PteNi metallic foam structured catalysts. *Int. J. Hydrogen Energy* **2022**, *48*, 11943–11955. [[CrossRef](#)]
30. Zhan, H.; Wang, J.; Xu, X. Catalytic decomposition of  $N_2O$  over  $Ni_xCo_{1-x}CoAlO_4$  spinel oxides prepared by sol-gel method. *J. Fuel. Chem. Technol.* **2015**, *43*, 81–87. [[CrossRef](#)]
31. Yan, L.; Ren, T.; Wang, X.; Ji, D.; Suo, J. Catalytic decomposition of  $N_2O$  over  $M_xCo_{1-x}Co_2O_4$  (M=Ni, Mg) spinel oxides. *Appl. Catal. B Environ.* **2003**, *45*, 85–90. [[CrossRef](#)]
32. Hu, X.; Wang, Y.; Wu, R.; Zhao, L.; Wei, X.; Zhao, Y. Effects of zirconia crystal phases on the catalytic decomposition of  $N_2O$  over  $Co_3O_4/ZrO_2$  catalysts. *Appl. Surf. Sci.* **2020**, *514*, 145892. [[CrossRef](#)]
33. Li, S.; Xia, L.; Li, J.; Liu, X.; Sun, J.; Wang, H.; Chi, Y.; Li, C.; Song, Y. Effect of alkaline earth metal doping on the catalytic performance of cobalt-based spinel composite metal oxides in  $N_2O$  decomposition. *J. Fuel Chem. Technol.* **2018**, *46*, 1377–1385. [[CrossRef](#)]
34. Kim, M.; Lee, S.; Ryu, I.; Jeon, M.; Moon, S.; Roh, H.; Jeon, S.G. Catalytic decomposition of  $N_2O$  over cobalt based spinel oxides: The role of additives. *Mol. Catal.* **2017**, *442*, 202–207. [[CrossRef](#)]

35. Abu-Zied, B.M.; Soliman, S.A.; Abdellah, S.E. Pure and Ni-substituted  $\text{Co}_3\text{O}_4$  spinel catalysts for direct  $\text{N}_2\text{O}$  decomposition. *Chin. J. Catal.* **2014**, *35*, 1105–1112. [[CrossRef](#)]
36. Meloni, E.; Martino, M.; Renda, S.; Muccioli, O.; Pullumbi, P.; Brandani, F.; Palma, V. Development of Innovative Structured Catalysts for the Catalytic Decomposition of  $\text{N}_2\text{O}$  at Low Temperatures. *Catalysts* **2022**, *12*, 1405. [[CrossRef](#)]
37. Ho, P.H.; Świrk, K.; De Luna, G.S.; Jabłońska, M.; Ospitali, F.; Di Renzo, F.; Delahay, G.; Fornasari, G.; Vaccari, A.; Palkovits, R.; et al. Facile coating of  $\text{Co}_3\text{O}_4$  on open-cell metallic foam for  $\text{N}_2\text{O}$  catalytic decomposition. *Chem. Eng. Res. Des.* **2022**, *188*, 166–178. [[CrossRef](#)]
38. Meloni, E.; Martino, M.; Pierro, M.; Pullumbi, P.; Brandani, F.; Palma, V. MW-Assisted Regeneration of 13X Zeolites after  $\text{N}_2\text{O}$  Adsorption from Concentrated Streams: A Process Intensification. *Energies* **2022**, *15*, 4119. [[CrossRef](#)]
39. Valentini, M.; Groppi, G.; Cristiani, C.; Levi, M.; Tronconi, E.; Forzatti, P. The deposition of  $\gamma\text{-Al}_2\text{O}_3$  layers on ceramic and metallic supports for the preparation of structured catalysts. *Catal. Today* **2001**, *69*, 307–314. [[CrossRef](#)]
40. Sing, K.S.W.; Everett, D.H.; Haul, R.A.W.; Moscou, L.; Pierotti, R.A.; Rouquerol, J.; Siemieniewska, T. Reporting physisorption data for gas/solid systems with special reference to the determination of surface area and porosity (Recommendations 1984). *Pure Appl. Chem.* **1985**, *57*, 603–619. [[CrossRef](#)]
41. Italiano, C.; Balzarotti, R.; Vita, A.; Latorrata, S.; Fabiano, C.; Pino, L.; Cristiani, C. Preparation of structured catalysts with Ni and Ni-Rh/ $\text{CeO}_2$  catalytic layers for syngas production by biogas reforming processes. *Catal. Today* **2016**, *273*, 3–11. [[CrossRef](#)]
42. Sadovszkaya, E.; Pinaeva, L.; Skazka, V.; Prosvirin, I. Kinetics of Oxygen Exchange and  $\text{N}_2\text{O}$  Decomposition Reaction over  $\text{MeO}_x/\text{CeO}_2$  (Me = Fe, Co, Ni) Catalysts. *Materials* **2023**, *16*, 929. [[CrossRef](#)] [[PubMed](#)]
43. Nabgan, W.; Abdullah, T.A.T.; Mat, R.; Nabgan, B.; Gambo, Y.; Moghadamian, K. Acetic acid-phenol steam reforming for hydrogen production: Effect of different composition of  $\text{La}_2\text{O}_3\text{-Al}_2\text{O}_3$  support for bimetallic Ni-Co catalyst. *J. Environ. Chem. Eng.* **2016**, *4*, 2765–2773. [[CrossRef](#)]

**Disclaimer/Publisher's Note:** The statements, opinions and data contained in all publications are solely those of the individual author(s) and contributor(s) and not of MDPI and/or the editor(s). MDPI and/or the editor(s) disclaim responsibility for any injury to people or property resulting from any ideas, methods, instructions or products referred to in the content.